Int. J. Heat Mass Transfer. Vol. 32, No. 1, pp. 105–120, 1989
Printed in Great Britain

0017–9310/89 $3.00 + 0.00

Variable density effects on axisymmetric sudden-expansion flows

G. J. YOO and R. M. C. SO
Department of Mechanical and Aerospace Engineering, Arizona State University, Tempe, AZ 85287, U.S.A.

(*Received* 1 *March* 1988 *and in final form* 3 *June* 1988)

Abstract—The flow through an axisymmetric sudden expansion is investigated numerically. A low-Reynolds-number full Reynolds stress closure that can account for viscous effects near a wall and thus avoids the use of wall functions is used to close the time-averaged Navier–Stokes equations. The calculated results are compared with recent laser Doppler measurements and show that the recirculating flow and reattachment behavior are correctly predicted by the low-Reynolds-number full Reynolds stress model. Since density variation complicates mixing, coaxial flow of two different gases into an axisymmetric sudden expansion is also investigated using the full Reynolds stress model, but with the model modified to account for variable density effects. The scalar field away from the wall is calculated by solving the modelled scalar flux transport equations, but in the near-wall region, the scalar field is approximated by a constant Schmidt number. Good agreement is obtained between predictions and measurements. However, the comparison indicates that the additional terms due to density variation in the momentum and scalar flux transport equations are of importance near a wall and the governing equations for the scalar field should be modified to account for near-wall viscous dissipation effects because turbulence in this region is not isotropic.

1. INTRODUCTION

TURBULENT flows through axisymmetric sudden expansions are influenced by many parameters. Among these are inlet flow Reynolds number, expansion ratio, step height, inlet geometry, inlet Mach number, inlet turbulence and inlet boundary layer. Reference [1] examined the relative importance of these parameters on the subsequent flow behavior downstream of the sudden expansion and found that inlet turbulence is the most important parameter affecting the reattachment length. The reason is that the higher inlet turbulence tends to energize the separating shear layer and this, in turn, causes the shear layer to spread faster and thus reattach sooner.

In the case of non-isothermal flows, the recirculation region downstream of the sudden expansion and the reattachment length are further affected by the thermal boundary conditions [2, 3]. Baughn *et al.* [3] found that when a constant wall heat flux boundary condition was imposed, the measured Nusselt number reached a minimum value at about one step height downstream of the expansion. They interpreted this to indicate the existence of a counterrotating secondary vortex in the corner region. It is speculated that this secondary vortex is turbulence driven rather than pressure driven. Later, careful measurements in the recirculation region of an isothermal, axisymmetric sudden-expansion flow using a laser Doppler anemometer clearly showed the existence of the counterrotating secondary vortex in the corner region [4, 5]. Therefore, the flow downstream of the sudden expansion is very complex. It involves recirculating flow, a counterrotating secondary vortex in the corner, shear layer reattachment, boundary layer development and rapid distortion of turbulence in the region surrounding the reattachment point. These complexities render the axisymmetric sudden-expansion flow very difficult to calculate and thus offer turbulence modellers a challenge to find a turbulence model that can replicate all the salient features of this flow.

Very often, the sudden-expansion geometry is used in dump-combustor designs. As a result, density variation, chemical reaction and heat release are important parameters affecting dump-combustor flows. If the dump combustor is used in ramjet projectiles, missile rotation will also influence the flow inside the ramjet combustor. Reference [5] investigated constant-density mixing in an axisymmetric sudden-expansion flow with and without system rotation. They found that rotation alone has a negative effect on the shear layer reattachment [5]. Their results showed that the reattachment length decreases linearly with increasing rotational speed. However, the corner vortex was still found to be rather prominent in the flow. Density variation in the flow also contributed to a decrease in the reattachment length [6]. Again, the corner vortex was observed to be present in the flow. Combined variable-density and rotation effects further decreased the reattachment length but failed to eliminate the corner vortex [6]. Therefore, it seems that the turbulence driven corner vortex is an important feature of the flow and the validity of any turbulence model for an axisymmetric sudden-expansion flow should be judged by its ability to reproduce this feature in the prediction.

Launder [7] showed how such an axisymmetric sudden-expansion flow can be calculated by adopting a parabolized sublayer model for the flow near the wall

NOMENCLATURE

a	density parameter, $1/\rho_h - 1/\rho_a$
b	density parameter, $1/\rho_a$
$C_1, C_3, C_4, C_5, C_s, C_{s\theta}, C_{1\theta}, C_{2\theta}, C_\mu, C_{\varepsilon 1}, C_{\varepsilon 2}$, $C_{\theta^2}, C_{D\theta^2}$	model constants
C, c	Favre mean and fluctuating helium volume concentration
c'	r.m.s. of c
C_{in}	inlet mean helium volume concentration
H	step height of sudden-expansion tube
k	turbulent kinetic energy, $\frac{1}{2}(\widetilde{u_i u_i})$
P	mean pressure
r	radial coordinate measured from tube centerline
R	radius of sudden-expansion tube
Sc, Sc_t	molecular and turbulent Schmidt number
U, u	Favre mean and fluctuating velocity along x-direction
$\bar{U}$	conventional time-averaged velocity along x-direction
U_{in}	inlet $\bar{U}$
U_0	U at tube centerline
u''	fluctuating part of Reynolds decomposition of instantaneous axial velocity
u'	r.m.s. of u''
u'_0	u' at tube centerline
u_τ	friction velocity
U_i, u_i	ith component of Favre mean and fluctuating velocity
v	radial Favre fluctuating velocity
w	circumferential Favre fluctuating velocity
w''	fluctuating part of Reynolds decomposition of instantaneous circumferential velocity
w'	r.m.s. of w''
x	axial coordinate measured from sudden-expansion inlet
x_i	ith component of coordinate
x_2	coordinate normal to the wall
x_r	reattachment length
y^+	wall coordinate, $\rho(R-r)u_\tau/\mu$.

Greek symbols

α	density ratio parameter, $\rho_h/\rho_a - 1$
$\alpha_1, \beta_1, \gamma_1$	model constants
γ, γ_t	molecular and turbulent diffusivity
ε	dissipation rate of k
Θ, θ	Favre mean and fluctuating mixture mass fraction
μ, μ_t	molecular and turbulent viscosity
ρ	instantaneous mixture density
$\bar{\rho}$	mean of ρ
ρ''	fluctuating part of ρ
ρ_a	air density
ρ_h	helium density
ρ_j	density of coaxial jet at sudden-expansion inlet
$\sigma_k, \sigma_\varepsilon$	model constants
τ_{ij}	Favre mean viscous stress tensor
ψ	stream function, $\int_0^r \bar{\rho}\bar{U}r\,dr$
ψ_0	ψ at tube centerline.

Overbars

$\bar{\ }$	denotes conventional (or Reynolds) time average
$\widetilde{\ }$	denotes density-weighted (or Favre) time average.

and matching this to a fully elliptic treatment outside of the wall layer. His calculations produced the secondary corner vortex, which has been observed experimentally [4–6] but has not been predicted in the past using wall functions [7]. Therefore, this provides strong arguments against the use of wall functions for this type of complex internal flows because they simply fail to reproduce the correct physics near the wall. Recently, Prud'homme and Elghobashi [8] proposed to calculate a non-isothermal axisymmetric sudden-expansion flow using a full Reynolds stress model for momentum transport and an algebraic closure for the thermal fluxes. They modified the near-wall models of Launder *et al.* [9] and Hanjalic and Launder [10] to account for low-Reynolds-number effects in the wall region and avoid the use of wall functions. However, their calculations were carried out from a location downstream of the sudden expansion, rather than at the inlet. Consequently, their results failed to show the existence of the corner vortex, even though the location of the minimum Nusselt number was predicted correctly. Besides, their model has one drawback and that is that the stress dissipation rates near a wall fail to approach their asymptotic values correctly.

Launder and Reynolds [11] proposed a near-wall dissipation rate model that approaches the asymptotic values correctly. Their model was incorporated into a low-Reynolds-number full Reynolds stress closure by Kebede *et al.* [12] who applied it to calculate flat plate boundary layer and periodic pipe flows. Their results were very encouraging but failed to give good agreement with periodic pipe flow data. Recently, ref. [13] proposed an alternative low-Reynolds-number full Reynolds stress model and compared its performance in the calculation of fully-developed turbulent pipe flow with that of Kebede *et al.*'s model [12]. The

two model predictions were found to be essentially identical. However, the model in ref. [13] was numerically relatively more stable near a wall; therefore, it is most suitable for complex flow calculations. Since then, the model [13] has been applied to calculate flows with wall transpiration [14] and behind a backward facing step [15]. The results clearly demonstrate the inadequacy of the wall functions for complex turbulent flows and the validity and applicability of the low-Reynolds-number model [13] for such flows. In view of these successes, the low-Reynolds-number model [13] is applied to calculate axisymmetric sudden-expansion flows with and without density variation.

In the above discussion, several salient features of sudden-expansion flows are pointed out. These are the secondary corner vortex and decreased reattachment length with increased inlet turbulence, increased system rotation and with variable-density mixing. A turbulence model is judged to be successful if it can replicate these and related features. The present objectives are two-fold. Firstly, to demonstrate the validity of the low-Reynolds-number model [13] for axisymmetric sudden-expansion flows. For given inlet conditions, the model is tested for its ability to predict the secondary vortex, the reattachment length, the behavior of the recirculating flow and the subsequent flow development downstream of reattachment. Secondly, the model is extended to calculate the effect of variable-density mixing. As a first attempt, the scalar field near the wall is modelled by the assumption of a constant Schmidt number. Away from the near-wall region, it is calculated by solving the modelled scalar flux transport equations. These calculations are compared to the recent laser Doppler and hot-wire measurements [5, 6]. This paper will not discuss the effects of inlet turbulence and system rotation because they are presently under investigation.

2. GOVERNING EQUATIONS AND TURBULENCE CLOSURE

Due to density variations, the density-weighted or Favre [16] decomposition is adopted in this study because the Reynolds decomposition yields additional contributions from density fluctuations which are difficult to model. It should be noted that, while the time-averaged value of the unweighted fluctuation is zero, that of the density-weighted fluctuation is not. Instead, the time-averaged value of the product of the density and the density-weighted fluctuation is zero.

If only stationary turbulent flows are considered, then the Reynolds governing equations for mass, momentum and mixture fraction written in Favre-averaged variables can be conveniently expressed in Cartesian tensor notation as [16]

$$\frac{\partial}{\partial x_i}(\bar{\rho}U_i) = 0 \tag{1}$$

$$\frac{\partial}{\partial x_j}(\bar{\rho}U_iU_j) = -\frac{\partial P}{\partial x_i} + \frac{\partial}{\partial x_j}\left(\mu\frac{\partial U_i}{\partial x_j} - \bar{\rho}\widetilde{u_iu_j}\right) \tag{2}$$

$$\frac{\partial}{\partial x_i}(\bar{\rho}U_i\Theta) = \frac{\partial}{\partial x_i}\left(\gamma\frac{\partial \Theta}{\partial x_i} - \bar{\rho}\widetilde{u_i\theta}\right). \tag{3}$$

The equations are not closed because of the presence of the terms $-\bar{\rho}\widetilde{u_iu_j}$ and $-\bar{\rho}\widetilde{u_i\theta}$.

Two different closures are proposed to close the equations and they are the full Reynolds stress and k–ε closures. For variable-density flows, the full Reynolds stress closure is provided by the solution of

$$\bar{\rho}U_k\frac{\partial\widetilde{u_iu_j}}{\partial x_k} = D_{ij}^{\mathrm{L}} + D_{ij}^{\mathrm{T}} + P_{ij} + \Phi_{ij} + G_{ij} + T_{ij} - \varepsilon_{ij} \tag{4}$$

$$\bar{\rho}U_k\frac{\partial\widetilde{u_i\theta}}{\partial x_k} = D_{i\theta}^{\mathrm{L}} + D_{i\theta}^{\mathrm{T}} + Q_{i\theta} + \Psi_{i\theta} + G_{i\theta} + T_{i\theta} - \varepsilon_{i\theta}. \tag{5}$$

The terms on the right-hand side of equations (4) and (5) represent molecular and turbulent diffusion, mean shear production, pressure redistribution, additional production (the G and T terms which are extra terms of interaction between the Favre-averaged fluctuating quantities and the gradients of the mean fields) and viscous dissipation of $\bar{\rho}\widetilde{u_iu_j}$ and $\bar{\rho}\widetilde{u_i\theta}$, respectively. These equations are not closed and models are required for D_{ij}^{T}, Φ_{ij}, ε_{ij}, $D_{i\theta}^{\mathrm{T}}$, $\Psi_{i\theta}$ and $\varepsilon_{i\theta}$. Even though the terms G_{ij}, T_{ij}, $G_{i\theta}$ and $T_{i\theta}$ involve $\tilde{u}_i$, $\tilde{\theta}$ and the gradients of the mean fields, they can be evaluated exactly and therefore do not need modelling. The approach taken to close the equations is based on the constant-density models for D_{ij}^{T}, Φ_{ij}, etc. and the assumption that these models, even though formulated within the unweighted framework, could be adopted without change for the Favre-averaged formulation. As a result, the suggestions of Jones [17] for variable-density flows are used to model the terms, D_{ij}^{T}, Φ_{ij}, $D_{i\theta}^{\mathrm{T}}$ and $\Psi_{i\theta}$, while the low-Reynolds-number dissipation model of ref. [13] is used to approximate ε_{ij}. Finally, $\varepsilon_{i\theta}$ is assumed to be zero because there is no first-order isotropic tensor.

If the diffusion model of Hanjalic and Launder [10] is modified for D_{ij}^{T}, Rotta's model [18] is extended to Φ_{ij}, Jones' model [17] is adopted for $D_{i\theta}^{\mathrm{T}}$ and Launder's model [19] is invoked for $\Psi_{i\theta}$, then the expressions for these terms can be written as

$$D_{ij}^{\mathrm{L}} = \frac{\partial}{\partial x_k}\left(\mu\frac{\partial\widetilde{u_iu_j}}{\partial x_k}\right) \tag{6}$$

$$D_{ij}^{\mathrm{T}} = \frac{\partial}{\partial x_k}\left[C_s\bar{\rho}\frac{k}{\varepsilon}\left(\widetilde{u_ku_l}\frac{\partial\widetilde{u_iu_j}}{\partial x_l} + \widetilde{u_ju_l}\frac{\partial\widetilde{u_ku_i}}{\partial x_l} + \widetilde{u_iu_l}\frac{\partial\widetilde{u_ju_k}}{\partial x_l}\right)\right] \tag{7}$$

$$\Phi_{ij} = -C_1\bar{\rho}\frac{k}{\varepsilon}\left(\widetilde{u_iu_j} - \tfrac{2}{3}\delta_{ij}k\right) \tag{8}$$

$$\varepsilon_{ij} = \tfrac{2}{3}\bar{\rho}\varepsilon\delta_{ij} + \frac{2\mu\delta_{il}\delta_{jm}\widetilde{u_i u_m}}{x_2^2} \tag{9}$$

$$D_{i\theta}^{L} = \frac{\partial}{\partial x_k}\left(\bar{\rho}(\gamma+\mu)\frac{\partial\widetilde{u_i\theta}}{\partial x_k}\right) \tag{10}$$

$$D_{i\theta}^{T} = \frac{\partial}{\partial x_k}\left[C_{s\theta}\bar{\rho}\frac{k}{\varepsilon}\left(\widetilde{u_k u_j}\frac{\partial\widetilde{u_i\theta}}{\partial x_j} + \widetilde{u_i u_j}\frac{\partial\widetilde{u_k\theta}}{\partial x_j}\right)\right] \tag{11}$$

$$\Psi_{i\theta} = -C_{1\theta}\bar{\rho}\frac{\varepsilon}{k}\widetilde{u_i\theta} + C_{2\theta}\bar{\rho}\widetilde{u_k\theta}\frac{\partial U_i}{\partial x_k}. \tag{12}$$

Also, the exact terms, P_{ij} and $Q_{i\theta}$, can be written as

$$P_{ij} = -\left[\bar{\rho}\widetilde{u_i u_k}\frac{\partial U_j}{\partial x_k} + \bar{\rho}\widetilde{u_j u_k}\frac{\partial U_i}{\partial x_k}\right]f_3 \tag{13a}$$

$$f_3 = \begin{cases} 1, & \text{when } i = j \\ 1-\exp\left[-C_5\bar{\rho}u_\tau x_2/\mu\right], & \text{when } i \neq j \end{cases} \tag{13b}$$

$$Q_{i\theta} = -\left[\bar{\rho}\widetilde{u_k\theta}\frac{\partial U_i}{\partial x_k} + \bar{\rho}\widetilde{u_i u_k}\frac{\partial\Theta}{\partial x_k}\right]. \tag{14}$$

The terms G_{ij}, $G_{i\theta}$, T_{ij}, and $T_{i\theta}$ contain $\tilde{u}_i$ and $\tilde{\theta}$ and represent interactions between the momentum and the scalar fields. They can be expressed in terms of $\widetilde{u_i\theta}$ and $\widetilde{\theta^2}$ by using the following relations. The time-averaged Favre fluctuating velocity and mixture fraction are given by

$$\tilde{u}_i = -\frac{\overline{\rho'' u_i}}{\bar{\rho}} \quad \text{and} \quad \tilde{\theta} = -\frac{\overline{\rho''\theta}}{\bar{\rho}}. \tag{15}$$

Since the mixture density can be expressed as

$$\frac{1}{\rho} = a(\Theta+\theta)+b \tag{16}$$

the fluctuating density can be shown to be given by

$$\rho'' = -a\bar{\rho}\rho\theta. \tag{17}$$

Therefore, combining eqns (15) and (17) gives

$$\tilde{u}_i = a\bar{\rho}\widetilde{u_i\theta} \quad \text{and} \quad \tilde{\theta} = a\bar{\rho}\widetilde{\theta^2}. \tag{18}$$

With these results, the G's and T's can be written out exactly as

$$G_{ij} = -\left[\tilde{u}_i\frac{\partial P}{\partial x_j} + \tilde{u}_j\frac{\partial P}{\partial x_i}\right] = -a\left[\bar{\rho}\widetilde{u_i\theta}\frac{\partial P}{\partial x_j} + \bar{\rho}\widetilde{u_j\theta}\frac{\partial P}{\partial x_i}\right] \tag{19}$$

$$T_{ij} = \tilde{u}_i\frac{\partial\tau_{jk}}{\partial x_k} + \tilde{u}_j\frac{\partial\tau_{ik}}{\partial x_k} = a\left[\bar{\rho}\widetilde{u_i\theta}\frac{\partial\tau_{jk}}{\partial x_k} + \bar{\rho}\widetilde{u_j\theta}\frac{\partial\tau_{ik}}{\partial x_k}\right] \tag{20}$$

$$G_{i\theta} = -\tilde{\theta}\frac{\partial P}{\partial x_i} = -a\bar{\rho}\widetilde{\theta^2}\frac{\partial P}{\partial x_i} \tag{21}$$

$$T_{i\theta} = \tilde{\theta}\frac{\partial\tau_{ij}}{\partial x_j} + \tilde{u}_i\frac{\partial}{\partial x_j}\left(\gamma\frac{\partial\Theta}{\partial x_j}\right) = a\bar{\rho}\widetilde{\theta^2}\frac{\partial\tau_{ij}}{\partial x_j} + a\bar{\rho}\widetilde{u_i\theta}\frac{\partial}{\partial x_j}\left(\gamma\frac{\partial\Theta}{\partial x_j}\right). \tag{22}$$

Equation (18) is nonzero for variable-density flows and provides the necessary interactions between the fluctuating velocity and scalar fields. Therefore, the terms G_{ij} and $G_{i\theta}$ can be interpreted as additional production due to mean pressure gradient and T_{ij} and $T_{i\theta}$ as the mean shear interactions with $\tilde{u}_i$ and $\tilde{\theta}$. Since $\tilde{\theta}$ is related to $\widetilde{\theta^2}$ by equations (18), an equation for $\widetilde{\theta^2}$ is also required in order to close the set of governing equations. The modelled equation for $\widetilde{\theta^2}$ is adopted from Jones [17], or

$$\bar{\rho}U_j\frac{\partial\widetilde{\theta^2}}{\partial x_j} = \frac{\partial}{\partial x_j}\left[\bar{\rho}\gamma\frac{\partial\widetilde{\theta^2}}{\partial x_j} + C_{\theta^2}\bar{\rho}\frac{k^2}{\varepsilon}\frac{\partial\widetilde{\theta^2}}{\partial x_j}\right] - 2\bar{\rho}\widetilde{u_j\theta}\frac{\partial\Theta}{\partial x_j} - 2C_{D\theta^2}\bar{\rho}\varepsilon\frac{\widetilde{\theta^2}}{k}. \tag{23}$$

Finally, one more equation for ε is required to close the set of governing equations. The low-Reynolds-number form of Chien's equation [20] is modified for variable-density flows to give

$$\bar{\rho}U_j\frac{\partial\varepsilon}{\partial x_j} = \frac{\partial}{\partial x_j}\left[\left(\mu+\frac{\mu_t}{\sigma_\varepsilon}\right)\frac{\partial\varepsilon}{\partial x_j}\right] + C_{\varepsilon 1}\frac{\varepsilon}{k}\tilde{P} - C_{\varepsilon 2}\bar{\rho}\frac{\varepsilon^2}{k}f_1 - \frac{2\mu\varepsilon}{x_2^2}\exp\left(-C_4\bar{\rho}u_\tau x_2/\mu\right) \tag{24a}$$

where

$$f_1 = 1 - \frac{2}{9}\exp\left[-\left(\frac{\bar{\rho}k^2}{6\mu\varepsilon}\right)^2\right] \tag{24b}$$

$$\tilde{P} = -\bar{\rho}\widetilde{u_i u_k}\frac{\partial U_i}{\partial x_k} - a\bar{\rho}\widetilde{u_i\theta}\frac{\partial P}{\partial x_i} + a\bar{\rho}\widetilde{u_i\theta}\frac{\partial\tau_{ik}}{\partial x_k} \tag{25}$$

$$\mu_t = c_\mu\bar{\rho}\frac{k^2}{\varepsilon}f_2 \tag{26a}$$

$$f_2 = 1-\exp\left[-\frac{C_3\rho u_\tau x_2}{\mu}\right]. \tag{26b}$$

On the other hand, the k–ε model is specified by the equations governing the transport of k and ε. Since the equation for ε is given by equation (24a), the governing equation for k needs to be developed. If equation (4) is contracted, an equation for k is obtained. The result is

$$\bar{\rho}U_j\frac{\partial k}{\partial x_j} = \frac{\partial}{\partial x_j}\left[\left(\mu+\frac{\mu_t}{\sigma_k}\right)\frac{\partial k}{\partial x_j}\right] + \tilde{P} - \bar{\rho}\varepsilon + \frac{2\mu k}{x_2^2}. \tag{27}$$

The k–ε equations together with the gradient transport assumption

$$-\bar{\rho}\widetilde{u_i u_j} = \mu_t S_{ij} - \frac{2}{3}\delta_{ij}\left[\bar{\rho}k + \mu_t\frac{\partial U_m}{\partial x_m}\right] \tag{28a}$$

$$S_{ij} = \frac{\partial U_i}{\partial x_j} = \frac{\partial U_j}{\partial x_i} \tag{28b}$$

$$-\widetilde{\bar{\rho} u_i \theta} = \frac{\mu_t}{Sc_t} \frac{\partial \Theta}{\partial x_i} \tag{29}$$

therefore, provide a closed set of equations for the solution of equations (1)–(3).

It should be pointed out that the modelled equation (5) for $\widetilde{\bar{\rho} u_i \theta}$ is only valid for high-Reynolds-number flows. Therefore, it cannot be used to calculate scalar transport near a wall. In the present study, the near-wall calculation of the scalar fluxes $\widetilde{\bar{\rho} u_i \theta}$ is given by equation (29). Beyond the near-wall region, $\widetilde{\bar{\rho} u_i \theta}$ are determined by solving equation (5). The velocity field is, of course, obtained by solving the modelled equation (4) for $\widetilde{\bar{\rho} u_i u_j}$ all the way to the wall. For constant-density flows, the scalar fluxes $\widetilde{\bar{\rho} u_i \theta}$ are identically zero and the closures discussed are the same as those considered in refs. [13–15].

The justifications of the models, equations (7)–(9), (11) and (12), for constant- and variable-density flows have been thoroughly discussed by other researchers [13–15, 17, 21]. Furthermore, the applicability and reliability of Rotta's model [18] for pressure redistribution have been demonstrated in refs. [13–15] for complex internal flows, and the validity of these models for isothermal, variable-density and reacting flows have been convincingly verified in refs. [21, 22]. Therefore, the above models can be used to assess variable-density effects in sudden-expansion flows. Finally, the model constants associated with the velocity field are taken from ref. [13], while the model constants associated with the scalar field are obtained from ref. [22].

Four closure schemes are considered and these are designated as H–k–ε, L–k–ε, H–$A1$ and $A1$. For the sake of clarity, the various models used to make up the different closures are summarized in Table 1.

3. SOLUTION TECHNIQUE

The boundary conditions for the velocity field can be specified as follows. At the wall, all velocity components, Reynolds stresses and the dissipation rate are zero, while the symmetry condition is specified along the tube centerline. The exit boundary conditions are specified to be zero gradient in the flow direction for all flow variables except pressure. As for the scalar field, the scalar flux at the wall is evaluated according to equation (29), while $\Theta = 0$ is assumed at the wall. Also, the symmetry condition is applied at the symmetry plane and $\partial/\partial x$ of the scalar field is set equal to zero at the exit.

The SIMPLE algorithm is used to solve the finite-difference equations numerically. A hybrid finite-differencing scheme and staggered grids are used. In order to solve the set of governing equations, a density and a pressure field are first assumed. The governing finite-difference equations are then iterated to give the flow field with the pressure field updated to satisfy the continuity equation. Meanwhile, the density is updated using intermediate mean concentration. This procedure is repeated until the continuity, momentum and mean scalar equations are simultaneously satisfied. This means that the residual mass, momentum and species concentration and the relative error of mean mixture density meet the prescribed convergence criterion of less than 0.5%.

A non-uniform grid with 51×56 grid points is used to resolve the flow in the region of interest. The proper choice of grid size has been examined in refs. [14, 15]. It was found that the most efficient and accurate spacing in the normal direction is 5 grid points in the region $0 \leqslant y^+ < 5$, 10–15 grid points in the region $5 < y^+ \leqslant 100$ and about 31–36 grid points from $y^+ = 100$ to the tube centerline. Furthermore, the studies found that with 56 grid points in the stream direction, the results are quite independent of grid spacings. The grid system is staggered for velocity and scalar quantities. Through this procedure, the

Table 1. Labelling of various turbulence closures

Closures	Modelled equations solved	Models					Wall functions?	
		D_{ij}^T	Φ_{ij}	ε_{ij}	$D_{i\theta}^T$	$\Psi_{i\theta}$	Velocity	Scalar
H–k–ε	(24) and (27) without viscosity terms, $f_1 = f_2 = 1$	—	—	—	—	—	Yes	Yes
L–k–ε	(24) and (27)	—	—	—	—	—	No	No
H–$A1$	(4), (5) and (24) without viscosity terms $f_1 = f_2 = f_3 = 1$	(7)	(8)	(9) with second term neglected	(11)	(12)	Yes	Yes
$A1$	(4), (5) and (24)	(7)	(8)	(9)	(11)	(12)	No	No

conservation principles are satisfied more realistically because finite-differencing is applied to the control volume rather than at a point.

In the present study, the calculations are carried out for both constant- and variable-density mixing in sudden-expansion flows. The constant-density flow case is examined first so that the best models can be identified by comparison with the measurements of ref. [5]. These models are then used to investigate the variable-density flow case and their performance assessed by comparing with the recent measurements of ref. [6].

4. CONSTANT-DENSITY SUDDEN-EXPANSION FLOW

The calculations are carried out for the axisymmetric sudden-expansion flow experiment of ref. [5] because detailed near-wall measurements in the recirculation region are available. A schematic of the test rig is shown in Fig. 1(a) and the dimensions are: tube diameter, $d_2 = 63.5$ mm; inlet nozzle diameter, $d_1 = 43.2$ mm; combustor length, $L_2 = 508$ mm; and inlet nozzle length, $L_1 = 63.5$ mm. These geometries, therefore, give an expansion ratio, $d_2/d_1 = 1.47$; combustor length to diameter ratio, $L_2/d_2 = 8$; and a step height, $H = 10.15$ mm. Uniform flow at the plane of the sudden expansion is produced by the inlet nozzle and the inlet centerline turbulence intensity, u_0'/U_{in}, is $\sim 5.7\%$ and $U_{in} = 10.6$ m s^{-1}. These are the conditions specified at the sudden-expansion inlet for the calculation. Other variables are estimated from the locally isotropic, equilibrium turbulence assumption. Once determined, the same set of inlet conditions are used for all model calculations.

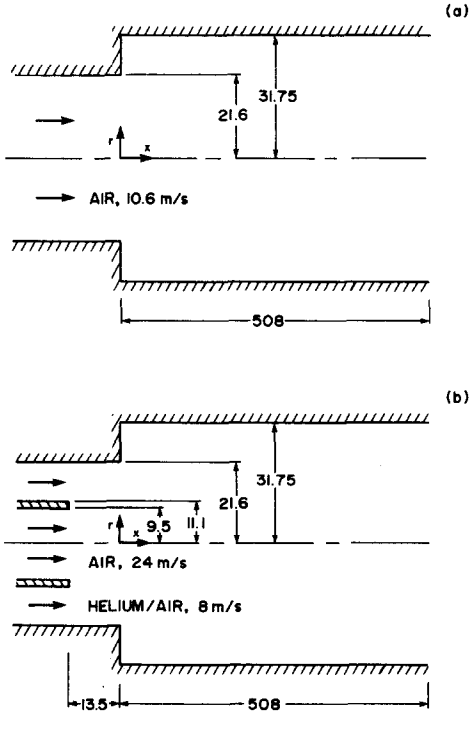

FIG. 1. Schematics of sudden-expansion geometries.

Altogether four model calculations are carried out for this experiment. These are the low- and high-Reynolds-number k–ε models, designated by L–k–ε and H–k–ε, respectively, and the low- and high-Reynolds-number full Reynolds stress models, designated by $A1$ and H–$A1$, respectively (Table 1). The governing equations for these models are equations (1)–(3) plus whatever additional equations are listed in Table 1. The high-Reynolds-number models (H–k–ε and H–$A1$) neglect all terms involving μ and $f_1 = f_2 = f_3 = 1$ are assumed. This means that the wall boundary conditions cannot be satisfied. Thus, wall functions have to be assumed for all flow variables. This is the biggest difference between the high- and low-Reynolds-number models. The comparison, therefore, attempts to answer the question, "Time to abandon wall functions?" posed by Launder [7] and to examine the relative merits of the L–k–ε and $A1$ models.

Selected results are plotted in Figs. 2–7 for comparison with the measurements of ref. [5]. The first three plots show the development of the flow variables, U, u' and $\overline{uv}$ in terms of r/R across the tube downstream of the sudden expansion. Calculations and measurements of U and u' in the recirculation region are given in Figs. 5 and 6. In these five plots, the top part shows the calculations using the H–k–ε and H–$A1$ models, while the bottom part depicts the results from the L–k–ε and $A1$ models. Therefore, this permits a comparison of the relative merits of all four models simultaneously without crowding the plots with too many similar curves. Finally, a comparison of the calculated and measured reattachment length is given in Fig. 7. The comparison is made on the basis of the locus of the zero mean velocity, or the $U = 0$ curve.

It can be seen that all four models predict U fairly well in the region away from the wall. The development of the mean flow in the tube core is correctly reproduced by the models considered (Fig. 2). However, such is not true for the turbulence field. The normal stress, u', is consistently overpredicted by the k–ε model and so is the shear field (Figs. 3 and 4). In the region immediately downstream of the sudden expansion, the u' and $\overline{uv}$ (Figs. 3 and 4) obtained from the k–ε models are nearly twice those calculated from the full Reynolds stress models (H–$A1$ and $A1$). It can be seen that the full Reynolds stress results are in better agreement with measurements. However, in the tube core region, both the low- and high-Reynolds-number models give essentially the same results.

Near the wall (Figs. 5 and 6), the picture is totally different. Firstly, there is a substantial difference between the high- and low-Reynolds-number model results and between the k–ε and the full Reynolds

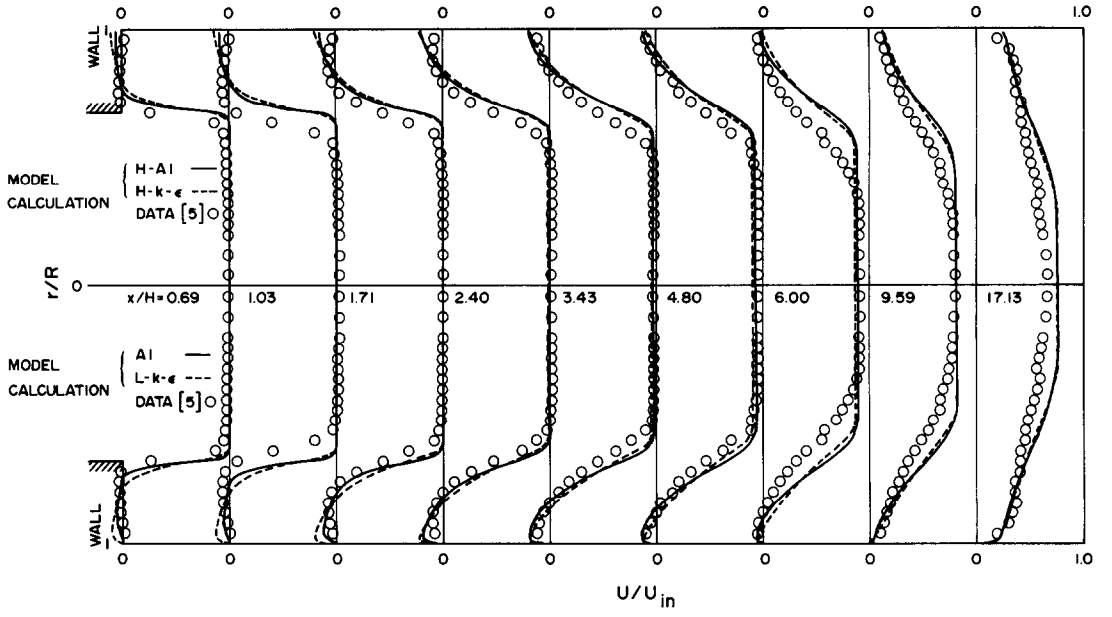

FIG. 2. Comparison of measured and calculated U in a constant-density sudden-expansion flow.

stress calculations. Experimental measurements show a secondary recirculation region near the corner, extending from $x/H = 0$ to ~ 1 in the stream direction and from $r/R = 1$ to ~ 0.9 in the radial direction. Both H–k–ε and H–$A1$ models fail to predict the secondary recirculation region. Furthermore, they give a flow behavior that is in total disagreement with measured flow. The L–k–ε results reveal such a secondary recirculation region; however, its predicted size is substantially smaller. On the other hand, the $A1$ model results are much more realistic. The axial extent of the secondary recirculation is correctly predicted by the $A1$ model but not the radial extent. Therefore, this further suggests that wall functions are not suitable for complex wall shear flows, and gives strong support to the proposal made by Launder [7].

Secondly, the k–ε models overestimate the maximum back-flow velocity. Its predicted magnitude is more than twice that calculated by the $A1$ models. As a result, the amount of reversed flow in the recirculation region is incorrectly estimated by the k–ε models. There is a substantial disagreement between the measured U's and those calculated using the $A1$ model in the region $x/H = 0$–1.28. However, agree-

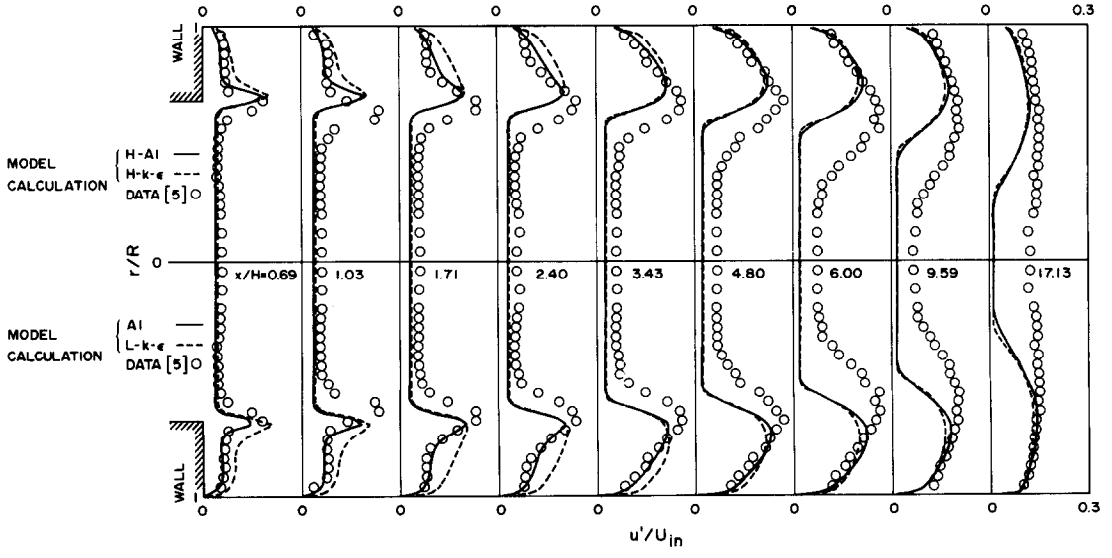

FIG. 3. Comparison of measured and calculated u' in a constant-density sudden-expansion flow.

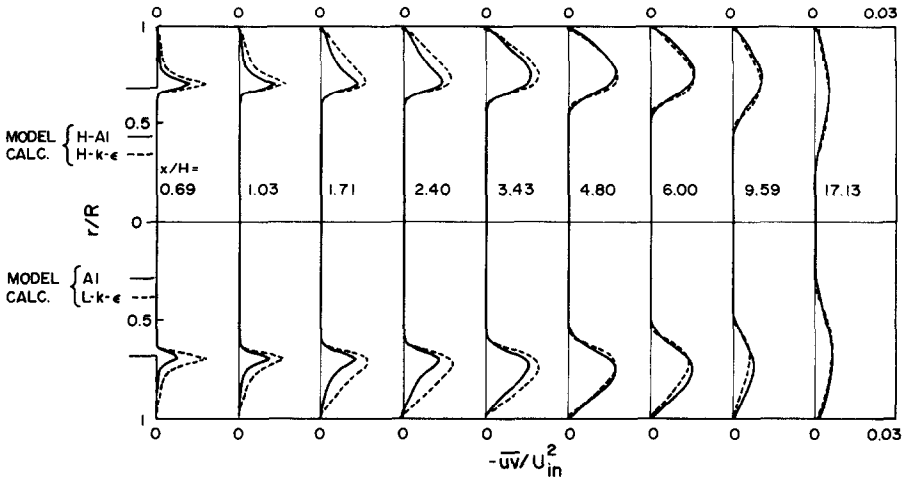

FIG. 4. Comparison of the calculated $\overline{uv}$ in a constant-density sudden-expansion flow.

ment improves downstream of $x/H = 1.28$. Overall, the $A1$ model gives the correct behavior of the flow in the recirculation region and shows that it is the model of choice for complex turbulent flows like the one considered here.

Finally, a comparison of the reattachment length further substantiates the conclusion drawn above concerning the $A1$ model (Fig. 7). It can be seen that the L–k–ε model over-predicts x_r while the H–k–ε and H–$A1$ models underestimate the reattachment length. The prediction by the L–k–ε model can be improved by varying the model constants. However, other flow properties are affected by changing the constants and the overall agreement with data is adversely affected. The same is also true of the H–k–ε and H–$A1$ models. Therefore, the $A1$ model gives the best prediction of the reattachment length and the flow in the recirculation region in general.

5. VARIABLE-DENSITY SUDDEN-EXPANSION FLOW

Consistent with the findings of ref. [15], the H–$A1$ model is found to be inadequate in the calculation of the near-wall flow in the recirculation region, especially in the prediction of the secondary vortex. Even though the L–k–ε model can predict the secondary vortex, its prediction of the reversed flow in the recirculation region is grossly in error. In spite of this, the L–k–ε model is also used to calculate the variable-density flow and its results compared with the calculations of the $A1$ model and the measurements of ref. [6]. In the L–k–ε model calculations, the scalar fluxes are evaluated from equation (29) with a Schmidt number $Sc_t = 0.8$ specified across the whole flow. The scalar variance $\widetilde{\theta^2}$ is obtained by solving equation (23) after a convergent solution has been obtained for the velocity and scalar fields. On the other hand, the $A1$ model calculations do not assume a constant Sc_t, except in the near-wall region (or $y^+ \leqslant 11$) where $Sc_t = 0.8$ is assumed. Outside of this region, the scalar fluxes are obtained by solving the transport equation (5). Again $\widetilde{\theta^2}$ is given by the solution of equation (23). Since the measurements of ref. [6] are given in terms of C and c', respectively, the calculated Θ and $\widetilde{\theta^2}$ have to be converted to C and c' for comparison with measurements. The following formulae are used to relate the statistics of the volume and mass fractions. These are

$$C = \frac{\Theta}{1+\alpha(1-\Theta)} \tag{30}$$

$$c' = \sqrt{\widetilde{c^2}} = \left[\frac{(1+\alpha C)^2\widetilde{\theta^2}}{(1+\alpha)^2}\right]^{1/2}. \tag{31}$$

Since the LDA measured velocities closely approximate the conventional or Reynolds time-averaged quantities, the calculated Favre-averaged velocities have to be converted to Reynolds-averaged quantities before comparison with measurements. The formulae used for $\bar{U}$ and u' are

$$\bar{U} = U - \frac{\overline{\rho''u''}}{\bar{\rho}} \tag{32}$$

$$u' = \left[\overline{u^2} + \frac{(\overline{\rho''u''})^2}{\bar{\rho}^2} - \frac{\overline{\rho''u''^2}}{\bar{\rho}}\right]^{1/2} \tag{33}$$

where $\overline{\rho''u''} = -\bar{\rho}\tilde{u}$ and $\tilde{u}$ is given by equations (18). Similar formulae can also be derived for the circumferential velocity. In the actual calculations of u' and w', the third-order correlations are neglected because they are assumed to be small compared to the other terms in equation (33). Therefore, the comparisons for the variable-density flow case are made with the measured $\bar{U}$, u', w', C and c'.

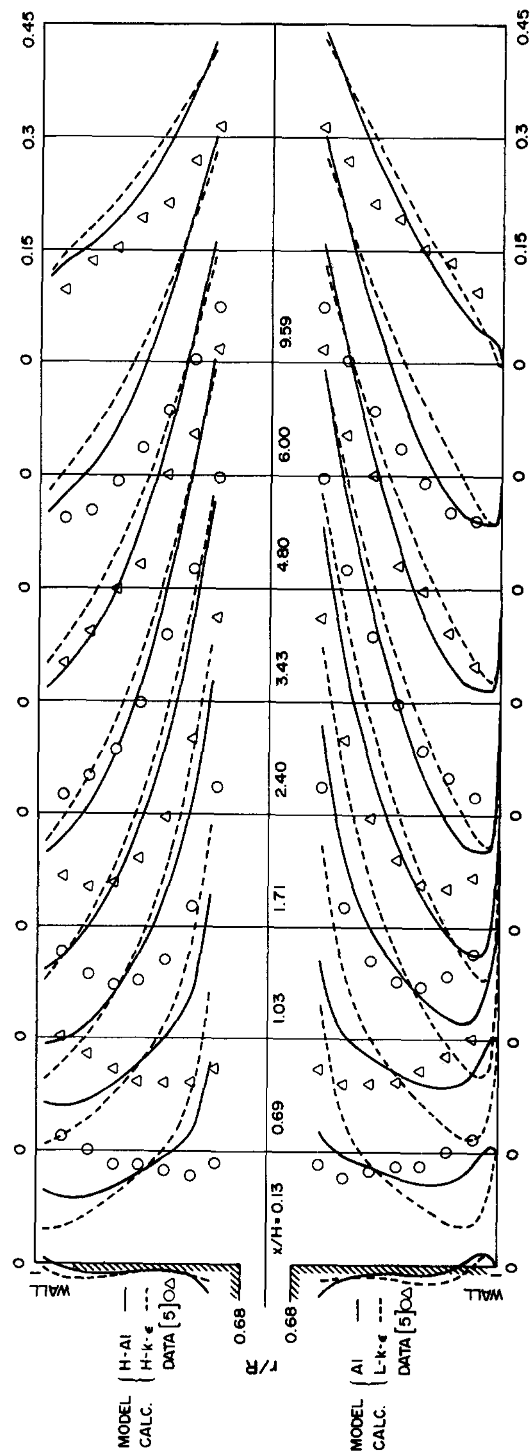

FIG. 5. Comparison of measured and calculated U in the recirculation region of a constant-density sudden-expansion flow.

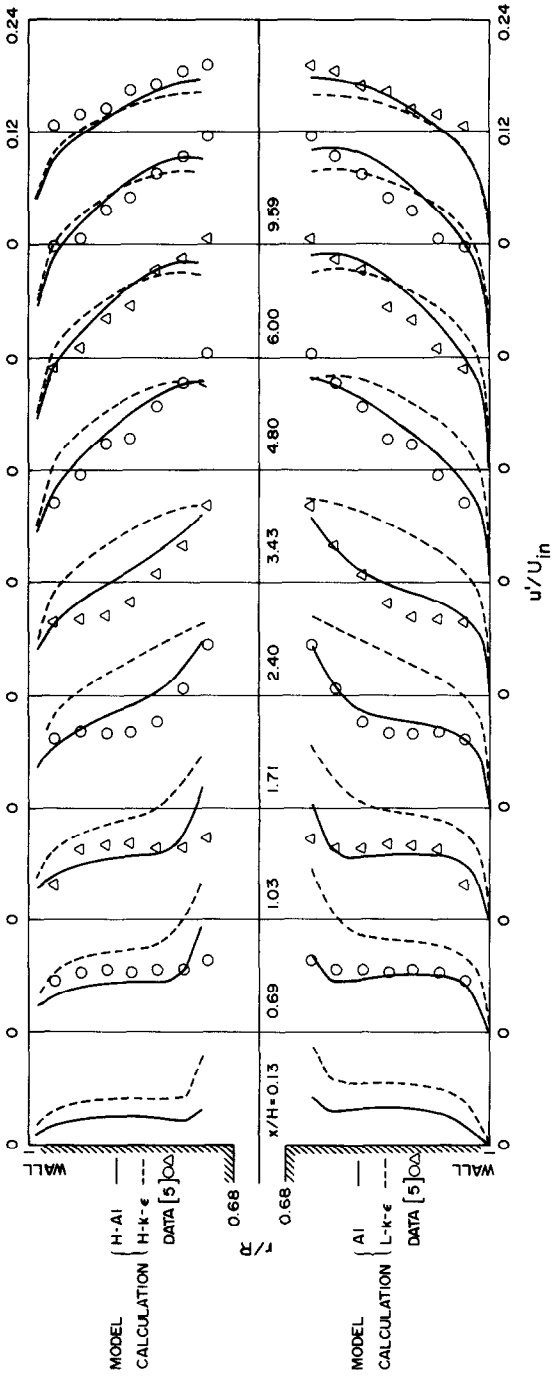

FIG. 6. Comparison of measured and calculated u' in the recirculation region of a constant-density sudden-expansion flow.

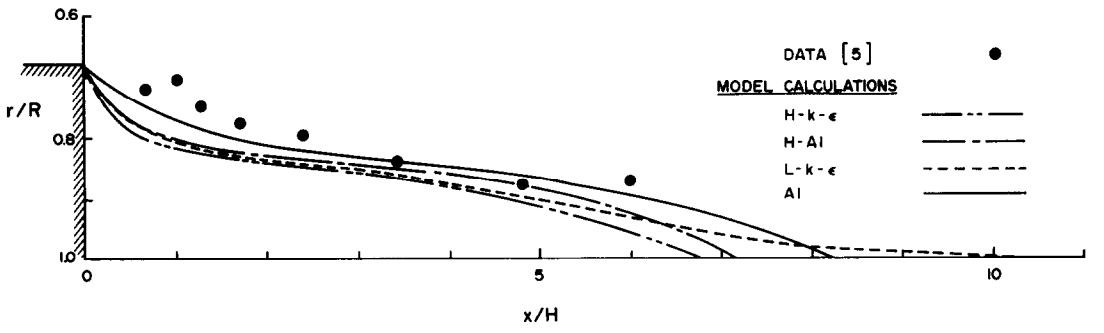

FIG. 7. Comparison of measured and calculated reattachment lengths.

A schematic of the sudden-expansion geometry of the experiments of ref. [6] is shown in Fig. 1(b). The dimensions of the inlet nozzle and sudden-expansion tube are the same as those of ref. [5]. However, the inlet geometry is quite different because a coaxial cylindrical tube is installed in the inlet nozzle. The dimensions of the coaxial tube are as shown in Fig. 1(b). Therefore, the sudden-expansion flow is made up of a coaxial flow of two different gases into an axisymmetric sudden expansion. The heavier gas (air) forms the inner jet while the lighter gas (helium/air mixture) forms the coaxial jet. The density ratio ρ_a/ρ_j is approximately 1.85, therefore, the inner jet is about twice as heavy as the coaxial jet. Reference [6] did not provide any measurements at $x = 0$. However, in the inlet region, measurements of C and c' were reported at $x/H = -1.33$ and 0.54 together with velocity data at $x/H = 0.54$. The inlet conditions at $x = 0$ are specified using experimental measurements and assuming the core flow to undergo a negligible change between $x/H = 0$ and 0.54, while the exit conditions are again assumed to be zero axial gradient for all flow variables except pressure.

The comparisons of the measured and calculated axial mean and r.m.s. fluctuating velocities normalized with the local centerline axial mean velocity are shown in Fig. 8. Generally, the agreement between predictions and data is good. The model exhibits the ability to predict the recirculating flow near the wall very well (Fig. 9). Just as in the constant-density flow case, a small region of counterrotating secondary vortex flow is again predicted by both the $A1$ and L–k–ε models. As before, the L–k–ε model overestimates the magnitude of the back-flow velocity and underestimates the extent of the secondary vortex. The r.m.s. velocities, u' and w', shown in Figs. 8–10 are obtained from the $A1$ model calculations only and again show good agreement with measurements. Clearly, the agreement near the wall is better than the rest of the flow region. Furthermore, the locations of the peaks in the shear layers are predicted correctly.

The predictions of the scalar concentration and its fluctuating field suffer from one major drawback. It is a lack of turbulent diffusion. The first region where insufficient diffusion is noticed is near the wall (Fig. 11). As a result, the helium volume concentration level in the recirculation region, especially immediately downstream of the sudden expansion, is incorrectly

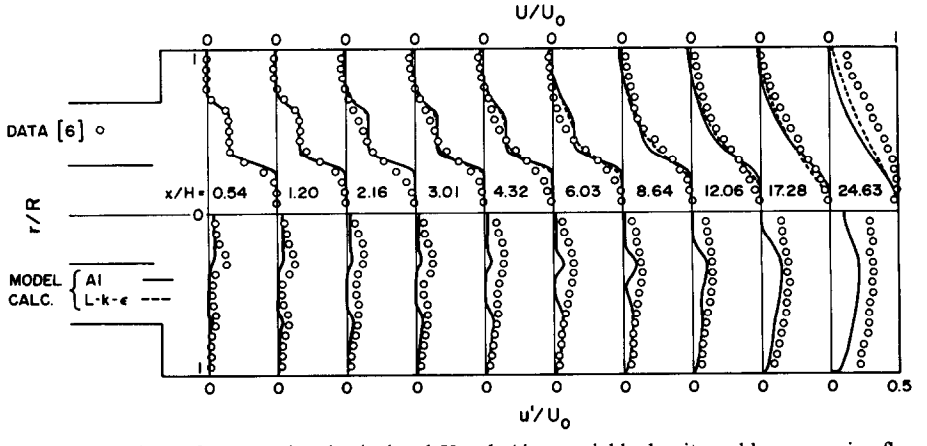

FIG. 8. Comparison of measured and calculated U and u' in a variable-density sudden-expansion flow.

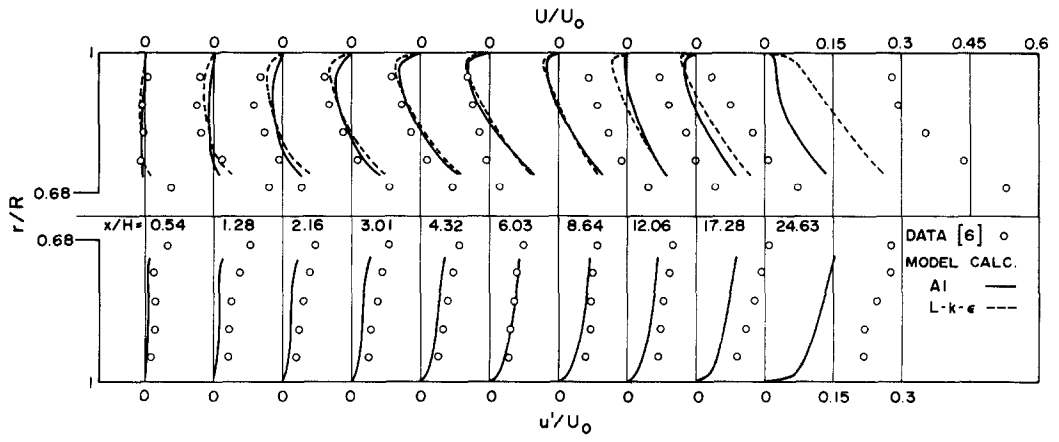

FIG. 9. Comparison of measured and calculated U and u' in the near-wall region of a variable-density sudden-expansion flow.

predicted. The lack of turbulent diffusion in this region is amply illustrated by the zero c' calculated. This could be due to the incorrect assumption of $Sc_t = 0.8$ in the near-wall region. Experimentally, the scalar fluctuation in this region is much higher and points to the fact that there is a lot of mixing activity within the recirculation region, even though the helium is trapped within this region and cannot escape across the dividing streamline. A second region where insufficient diffusion occurs is the region surrounding the mixing layer emanating from the inner tube. This leads to over-prediction of the peak in c' and under-prediction of C near the tube centerline (Fig. 12). The incorrect prediction could be remedied by modifying $C_{s\theta}$ in equation (11) to increase turbulent diffusion of $\widetilde{u_i\theta}$.

In order to further pursue the argument that the assumption $Sc_t = 0.8$ in the near-wall region is responsible for the lack of scalar diffusion near the wall, a second calculation was carried out with $Sc_t = 0.4$. The results of C and c' are also shown in Figs. 11 and 12 for comparison with the other calculations. Since the calculated velocity field is not affected by the near-wall Schmidt number assumed, the velocity results for the $Sc_t = 0.4$ case are not shown in Figs. 8–10. The mean C is not affected by a change of Sc_t in the near-wall region. However, the calculated c' clearly shows the effects of Sc_t, especially in the downstream region. Clearly, a lower value of Sc_t promotes scalar diffusion and, therefore, results in a more uniform distribution of c' in the region downstream of the reattachment point. It is also clear that a constant Sc_t assumption is not valid for this flow, because the model fails to account for the rapid diffusion of helium near the wall. This suggests that the scalar flux transport equation (5) should be modified to account for viscous dissipation effects near a wall. In other words, a low-Reynolds-number model similar to that proposed for equation (4) should be developed for equation (5). This will eliminate the necessity of invoking equation (29) to calculate $-\bar{\rho}\widetilde{u_i\theta}$ near a wall.

The importance of the additional terms G_{ij}, T_{ij}, $G_{i\theta}$ and $T_{i\theta}$ in the model calculations is also investigated. This was carried out by repeating the $A1$ model calculations with $Sc_t = 0.8$ but with the terms G_{ij}, T_{ij}, $G_{i\theta}$ and $T_{i\theta}$ neglected from equations (4) and (5). The resultant closure is therefore identical to that examined in refs. [13–15]; however, the flow properties calculated are density-weighted rather than unweighted. In view of this similarity, the comparison of the calculations with and without the additional

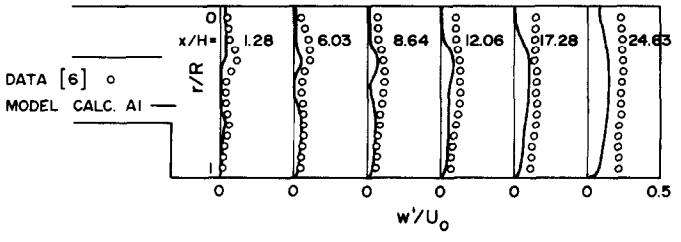

FIG. 10. Comparison of measured and calculated w' in a variable-density sudden-expansion flow.

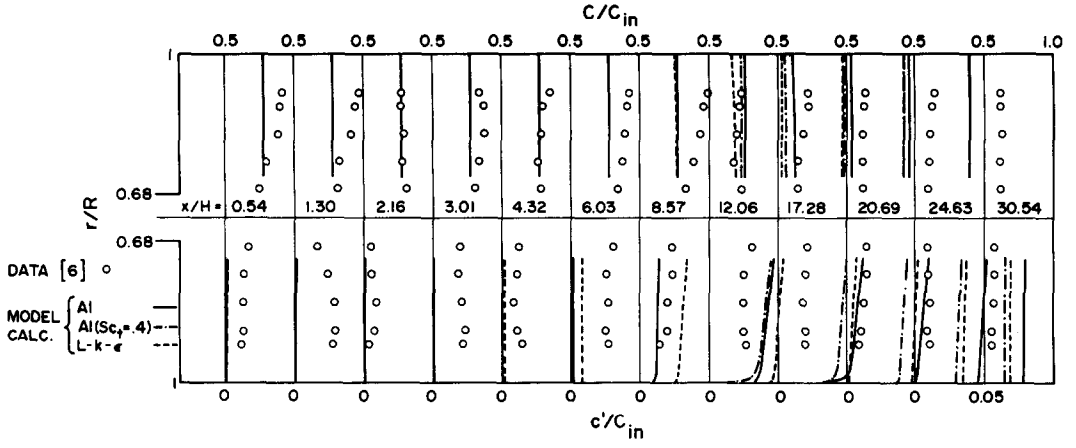

FIG. 11. Comparison of measured and calculated C and c' in the near-wall region.

terms will provide evidence to verify the applicability of constant-density models for variable-density flows. The results are best summarized by a comparison of the stream function plots for the sudden-expansion flow. A comparison of the calculated and measured ψ is shown in Fig. 13. In this plot, the calculated results are drawn from the $A1$ model with the additional terms retained in equations (4) and (5). The calculated ψ's drawn from the results of the L–k–ε and $A1$ models with the additional terms neglected in equations (4) and (5) are shown in Fig. 14. If the terms G_{ij}, T_{ij}, $G_{i\theta}$ and $T_{i\theta}$ in equations (4) and (5) are neglected, the resulting ψ plot shows little or no difference with the previous results (cf. Figs. 13 and 14). Both calculations, however, give an incorrect prediction of the reattachment length. The L–k–ε results are also consistent with the other model calculations. Again the predicted reattachment length is not in agreement with measurement. In general, all closures examined reproduce the qualitative behavior of the sudden-expansion flow correctly but give an incorrect prediction of the reattachment point (Fig. 13). Therefore, these results indicate that a direct extension of the constant-density models to variable-density flows is valid but insufficient.

6. CONCLUSIONS

The salient features of axisymmetric sudden-expansion flows with and without variable-density effects are correctly predicted by the low-Reynolds-number models considered. Some of these features are the existence of a counterrotating secondary vortex at the corner, reattachment of the separating shear layer and its subsequent development as a boundary layer and rapid distortion of turbulence in the region surrounding the reattachment point. These features are reproduced quite well by the $A1$ model and not as well by the L–k–ε model in the constant-density flow case. The agreement is quantitative for the $A1$ model

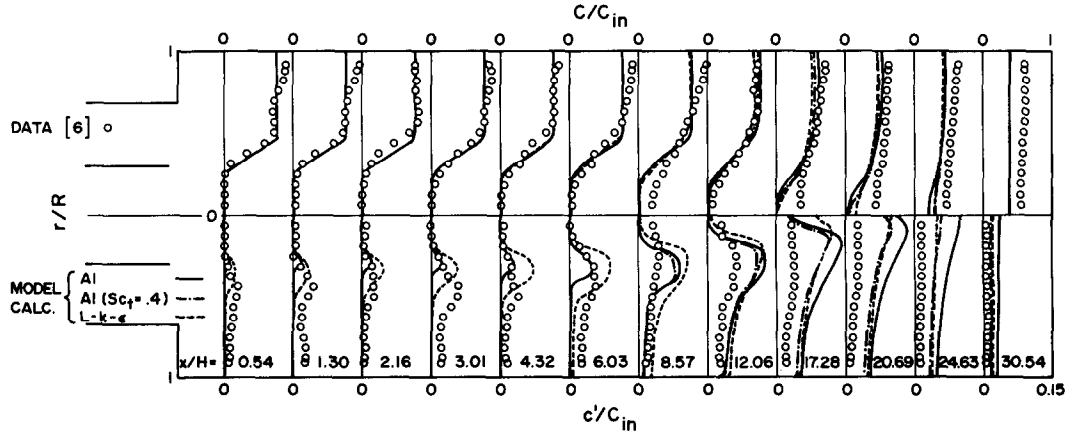

FIG. 12. Comparison of measured and calculated C and c' in a sudden-expansion flow.

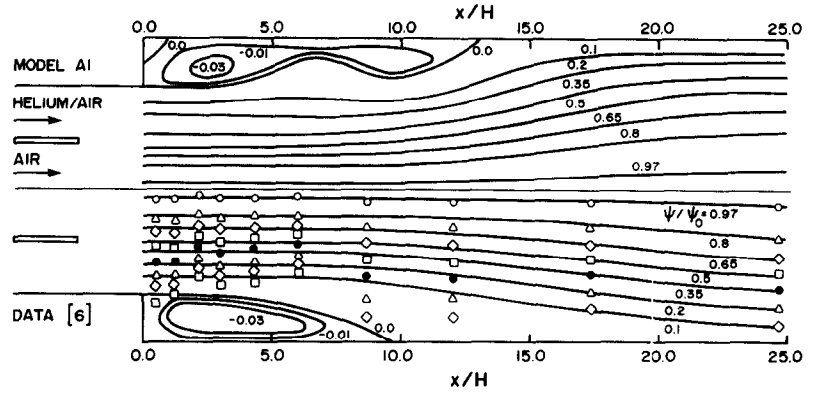

FIG. 13. Comparison of calculated and measured ψ's. The calculated ψ is obtained from the $A1$ model.

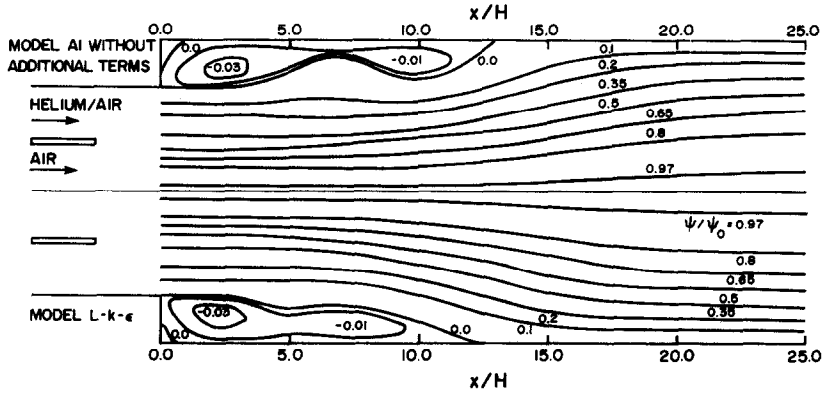

FIG. 14. Comparison of calculated ψ from the L–k–ε and $A1$ models. The G_{ij}, T_{ij}, $G_{i\theta}$ and $T_{i\theta}$ terms in the $A1$ model are neglected.

but it is more qualitative for the L–k–ε model because the L–k–ε model over-predicts the back flow and u' in the recirculation region. Also, the L–k–ε model overestimates the reattachment length. In the variable-density flow case, the agreement is more qualitative than quantitative for both the $A1$ and L–k–ε models. The reasons could be due to the assumption of a constant Schmidt number over the whole field for the L–k–ε model and in the near-wall region only for the $A1$ model and an incorrect specification for $C_{s\theta}$. As a result of this assumption, turbulent diffusion in the recirculation region as well as around the mixing layers emanating from the inner tube is grossly underpredicted. On the other hand, the additional terms due to $\bar{u}_i$ and $\bar{\theta}$ in the momentum and scalar flux transport equations are found to have little effect on the calculated properties, except in the near-wall region. The gross features of the flow are equally well predicted by the $A1$ model with or without the additional variable-density terms. In both cases, the recirculation region is incorrectly predicted. Therefore, the present results suggest that the scalar flux transport equations should also be modified to account for viscous effects near a wall just as in the transport equations for the Reynolds stresses. Furthermore, a direct extension of the constant-density models to variable-density flows is found to be valid but insufficient.

Acknowledgement—Research support from Naval Weapons Center under contract No. N60530-85-C-9001 is gratefully acknowledged.

REFERENCES

1. R. M. C. So, Inlet centerline turbulence effects on reattachment length in axisymmetric sudden-expansion flows, *Expl Fluids* **5**, 424–426 (1987).
2. K. M. Krall and E. M. Sparrow, Turbulent heat transfer in the separated, reattached and redevelopment regions of a circular tube, *J. Heat Transfer* **88**, 131–136 (1966).
3. J. W. Baughn, M. A. Hoffman, R. K. Takahashi and B. E. Launder, Local heat transfer downstream of an abrupt expansion in a circular channel with constant wall heat flux, *J. Heat Transfer* **106**, 789–796 (1984).
4. R. P. Durrett, W. H. Stevenson and H. D. Thompson, Radial and axial turbulent flow measurements with an

LDA in an axisymmetric sudden expansion air flow, ASME Special Publication **FED-33,** 127–133 (1985).
5. R. M. C. So and S. A. Ahmed, Rotation effects on axisymmetric sudden-expansion flows, *J. Prop. Pwr* **4,** 270–276 (1988).
6. R. M. C. So, M. H. Yu, M. V. Otugen and J. Y. Zhu, Rotation effects on inhomogeneous mixing in axisymmetric sudden-expansion flows, *Int. J. Heat Mass Transfer* **30,** 2411–2421 (1987).
7. B. E. Launder, Numerical computation of convective heat transfer in complex turbulent flows: time to abandon wall functions?, *Int. J. Heat Mass Transfer* **27,** 1485–1491 (1984).
8. M. Prud'homme and S. Elghobashi, Turbulent heat transfer near the reattachment of flow downstream of a sudden pipe expansion, *Numer. Heat Transfer* **10,** 349–368 (1986).
9. B. E. Launder, G. J. Reece and W. Rodi, Progress in the development of a Reynolds stress turbulence closure, *J. Fluid Mech.* **68,** 537–566 (1975).
10. K. Hanjalic and B. E. Launder, Contributions towards a Reynolds-stress closure for low-Reynolds-number turbulence, *J. Fluid Mech.* **74,** 593–610 (1976).
11. B. E. Launder and W. C. Reynolds, Asymptotic near-wall stress dissipation rates in a turbulent flow, *Physics Fluids* **26,** 1157–1158 (1983).
12. W. Kebede, B. E. Launder and B. A. Younis, Large amplitude periodic pipe flow: a second-moment closure study, *Proc. 5th Turbulent Shear Flows Symp.*, Paper No. 16 (1985).
13. R. M. C. So and G. J. Yoo, On the modelling of low-Reynolds-number turbulence, NASA CR-3994 (1986).
14. R. M. C. So and G. J. Yoo, Low-Reynolds-number modelling of turbulent flows with and without wall transpiration, *AIAA J.* **25,** 1556–1564 (1987).
15. R. M. C. So, Y. G. Lai, B. C. Hwang and G. J. Yoo, Low-Reynolds-number modelling of flows over a backward-facing step, *ZAMP* **39,** 13–27 (1988).
16. A. Favre, Statistical equations of turbulent gases. In *Problems of Hydrodynamics and Continuum Mechanics*, pp. 231–266. SIAM (1969).
17. W. P. Jones, Models for turbulent flows with variable density and combustion. In *Prediction Method for Turbulent Flows* (Edited by W. Kollman), pp. 379–422. Hemisphere, London (1980).
18. J. C. Rotta, Statistische Theorie Nichthomogener Turbulenz, *Zt. Phys.* **129,** 547–572 (1951); **131,** 51–77 (1951).
19. B. E. Launder, On the effect of gravitational field on the turbulent transport of heat and momentum, *J. Fluid Mech.* **69,** 569–581 (1975).
20. K. Y. Chien, Predictions of channel and boundary-layer flows with a low-Reynolds-number turbulence model, *AIAA J.* **20,** 33–38 (1982).
21. M. Nikjooy and R. M. C. So, On the modelling of scalar and mass transport in combustor flows, submitted to *Int. J. Numer. Meth. Engng.*
22. M. Nikjooy, R. M. C. So and R. E. Peck, Modelling of jet- and swirl-stabilized reacting flows in axisymmetric combustors, *Combust. Sci. Technol.* **58,** 135–153 (1988).

EFFETS DE LA MASSE VOLUMIQUE VARIABLE SUR DES ECOULEMENTS EN EXPANSION BRUSQUE AXISYMETRIQUE

Résumé—On étudie numériquement l'écoulement à travers un élargissement brusque axisymétrique. Une fermeture de tension de Reynolds qui tient compte des effets visqueux près de la paroi évite l'utilisation des fonctions de paroi et complète les équations de Navier–Stokes. Les résultats calculés sont comparés à des mesures récentes laser Doppler et ils montrent que l'écoulement de recirculation et le rattachement sont correctement prédits par ce modèle. Celui-ci est utilisé avec une modification pour tenir compte des effets de masse volumique variable. Le champ scalaire est calculé en résolvant les équations de transport pour la région écartée de la paroi, et près de la paroi le champ scalaire est approché par un nombre de Schmidt constant. Un bon accord est obtenu entre les calculs et les mesures. Néanmoins, la comparaison indique que les termes additionnels relatifs à la variation de masse volumique dans les équations de quantité de mouvement et de transport scalaire sont importants près de la paroi, et que les équations pour le champ scalaire doivent être modifiées pour tenir compte des effets de dissipation visqueuse près de la paroi, parce que la turbulence n'est pas isotrope dans cette région.

EINFLUSS VON DICHTEÄNDERUNGEN AUF ACHSENSYMMETRISCHE STRÖMUNGEN BEI PLÖTZLICHER EXPANSION

Zusammenfassung—Es wird eine achsensymmetrische Strömung bei plötzlicher Expansion numerisch untersucht. Die zeitgemittelten Navier–Stokes-Gleichungen werden mit Hilfe einer besonderen Schließbedingung gelöst, die Reibungs-Effekte in Wandnähe berücksichtigt und so die Benutzung von Wandfunktionen vermeidet. Die Schließbedingung enthält den turbulenten Impulsaustausch bei kleinen Reynolds-Zahlen. Die Rechenergebnisse werden mit neuen Laser-Doppler-Messungen verglichen. Es zeigt sich, daß die Rückströmung und das Verhalten beim Wiederanlegen der Strömung durch das Modell richtig, berechnet werden. Da Dichteänderungen die Mischung erschweren, wird auch eine koaxiale Strömung zweier Gase mit einer achsensymmetrischen plötzlichen Expansion mit dem Modell untersucht, das jedoch verändert wurde, um die Dichteänderungen zu berücksichtigen. Das Skalarfeld in Wandferne wird durch die Lösung der skalaren Transportgleichungen berechnet, während es in Wandnähe durch eine konstante Schmidt-Zahl angenähert wird. Es wird eine gute Übereinstimmung zwischen Rechnung und Messung erzielt. Der Vergleich zeigt jedoch, daß die zusätzlichen Terme zur Berücksichtigung der Dichteänderungen in den Transportgleichungen in Wandnähe wichtig sind und daß die Bilanzgleichungen für das Skalarfeld verändert werden sollten, um wandnahe viskose Dissipationseffekte zu berücksichtigen, da die Turbulenz in diesem Bereich nichtisotrop ist.

ВЛИЯНИЕ ПЕРЕМЕННОЙ ПЛОТНОСТИ НА ОСЕСИММЕТРИЧНЫЕ ВНЕЗАПНО РАСШИРЯЮЩИЕСЯ ТЕЧЕНИЯ

Аннотация—Численно исследуется течение через осесимметричное внезапное расширение канала. Для замыкания усредненных по времени уравнений Навье–Стокса используется модель полного Рейнольдсовского напряжения для низких чисел Рейнольдса, которая позволяет рассчитать эффекты вязкости вблизи стенки и таким образом не прибегать к использованию пристеночных функций. Полученные результаты сравнены с недавними лазер-Допплеровскими измерениями, и показано, что рециркулирующее течение и характер повторного присоединения правильно определены. Поскольку вариации плотности затрудняют смешивание, рассмотрено также соосное течение двух различных газов в осесимметричном внезапном расширении в рамках модели полного Рейнольдсовского напряжения, модифицированной с целью учета эффекта перемеменной плотности. Скалярное поле вдали от стенки определяется из решения модельных уравнений переноса скалярного потока, а в пристенной области скалярное поле аппроксимируется постоянным числом Шмидта. Получено хорошее соответствие между расчетами и измерениями. Однако сравнение обнаруживает, что вблизи стенки из-за переменной плотности необходимы дополнительные члены в уравнениях переноса импульса и скалярного потока и что определяющие уравнения для скалярного поля должны быть модифицированы с целью учета эффекта пристенной вязкой диссипации, так как в этой области турбулентность неизотропна.